



OPEN Dust distribution characteristics of the breathing zone in the walkway area of fully-mechanized mining face: a case study

Wei Zhang^{1,2,4}, Qingyi Tu^{3,5}✉, Sheng Xue^{3,4}, Fei Xing⁴, Xingxing Xu⁴, Zuheng Zhao⁵ & Chao Li⁶

To understand the dust distribution characteristics of fully mechanized mining faces, this study utilized the gravimetric method to sample dust in the walkway area during the coal cutting process of the shearer, followed by testing and analysis of the dust samples. The research findings reveal that the pollution level in the walkway area significantly surpasses coal mine safety regulations. There is no significant correlation between variations in dust concentration and dust quantity at different locations, with the region within 6 m behind the shearer exhibiting the highest dust quantity. The rate of change in respirable dust quantity is notably lower than that of non-respirable dust quantity. In all areas except those corresponding to the shearer, the number of dust particles within the range of 0 to 10 μm exceeds 90%. Additionally, dust particles on the mining face have smooth surfaces but are predominantly elongated in shape. These findings underscore the current inadequacies in effectively controlling dust in walkway areas. Therefore, there is a pressing need to implement more technological measures to control dust in these areas, with a specific emphasis on reducing the quantity of respirable dust, rather than solely focusing on variations in dust concentration.

Keywords Mining face, Walkway area, Dust concentration, Particle size distribution, Dust shape

Coal dust consists of fine particles generated during coal seam mining, primarily due to the fragmentation of coal by mining machines. Its formation is influenced by multiple factors¹. When suspended in the air at sufficient concentrations, coal dust can ignite upon exposure to open flames or electrical sparks, leading to an explosion. The minimum ignition temperature of dust under standard conditions is approximately 610 °C, with the lower explosion limit around 20–60 g/m³ and the upper explosion limit approximately 2000–6000 g/m³. Additionally, coal dust can contribute to gas-induced explosions², posing significant challenges to underground safety operations. With enhanced safety management by coal mining companies, accidents caused by coal dust explosions have become less frequent³. However, as the mechanization level and mining intensity of fully-mechanized mining faces increase, the amount of coal dust generated at the working face also rises, especially respirable dust⁴. The health problems associated with coal dust exposure have gradually become apparent. Prolonged exposure to high concentrations of coal dust can lead to diseases such as pneumoconiosis or silicosis, ultimately resulting in fatalities⁵. Public data indicates that as of 2021, China has reported a cumulative total of 915,000 cases of occupational pneumoconiosis⁶, with an increase of 11,809 cases in 2021 alone⁷, most of which are coal worker pneumoconiosis (CWP), not accounting for unreported cases. According to the *Coal Mine Safety Regulations* issued by the Ministry of Emergency Management of the People's Republic of China, the permissible limits for total dust concentration and respirable dust concentration are 4 mg/m³ and 2.5 mg/m³, respectively⁸. In contrast, the occupational exposure limits for respirable coal dust in the United States and Australia are 3 mg/m³ and 2 mg/m³, respectively⁹. However, some current measurement data indicate that coal dust concentrations during coal mining or tunneling activities far exceed these regulations^{10,11}. With the development of the concept

¹Guizhou Energy Group Corporation Limited, Guiyang 550000, China. ²Guizhou Research Institute of Coal Mine Design Co., LTD, Guiyang 550000, China. ³Joint National-Local Engineering Research Centre for Safe and Precise Coal Mining, Anhui University of Science and Technology, Huainan 232001, China. ⁴School of Safety Science and Engineering, Anhui University of Science and Technology, Huainan 232001, China. ⁵State Key Laboratory of Mining Response and Disaster Prevention and Control in Deep Coal Mines, Anhui University of Science and Technology, Huainan 232001, China. ⁶Hongliulin Mining Co., Ltd, Shaanxi Coal and Chemical Industry Group Co., Ltd, Shenmu 719300, China. ✉email: 13775889470@163.com

of occupational health in China, attention to coal dust control has also gradually increased¹². Due to space constraints at the mining face, completely avoiding contact between workers and dust is challenging. Therefore, understanding the extent and distribution characteristics of dust pollution is beneficial for efficient dust control and holds significant importance for mitigating coal dust explosions¹³.

Some scholars analyze the distribution characteristics of coal dust through on-site measurements. For instance, Nie et al.¹⁴ conducted comprehensive sampling of intake airways, return airways, and mining faces in a coal mine in Jincheng, Shanxi, with a particular focus on the variations in concentrations of PM 2.5 and PM 10. Guo et al.¹⁵ measured dust concentrations in walkway areas of a specific working face and divided them into two zones based on dust concentration variations. Apart from on-site measurements, some researchers attempt to study the distribution of coal mine dust in airflow through experiments. However, constructing an experimental model that faithfully replicates real-life conditions in a 1:1 scale is challenging. Although some experimental studies on coal mining faces have made progress^{16,17}, these studies have limitations in terms of constructing similar models, theories, and dimensions, making it difficult to apply their results to on-site dust control or further research. Furthermore, in theoretical research, early scholars treated dust as a gas phase and studied the variation in dust concentrations along the roadway by solving convection–diffusion equations^{18–20}. With the improvement in computer computational power, computational fluid dynamics (CFD) has gradually been applied to the study of gas–solid two-phase flow in coal mines^{21,22}. The Eulerian–Lagrangian approach is the primary research method for studying the diffusion and transport of dust in roadways. In these studies, airflow is considered a continuous phase, while dust is considered a discrete phase. The movement of dust in the flow field is analyzed by solving the Navier–Stokes equations and the particle force equation^{23–28}. Regardless of the method employed, scholars are more concerned with the dust distribution characteristics across the entire mining face or roadway, especially when using the CFD method for research. The National Institute for Occupational Safety and Health (NIOSH) supports the use of the hierarchy of controls to manage coal mine dust^{29,30}. However, current dust control efforts are still primarily focused on engineering controls or personal protective measures. For underground coal mines with limited space and complex mining conditions, there are still many challenges to achieving comprehensive dust control¹².

Hence, in the quest to reduce exposure to dust, current research should pay heightened attention to the spatial distribution of coal dust in the daily activity areas of coal miners, particularly in the breathing zone within the walkway area at a height of 1.5 m³¹. Dust concentrations at this level directly impact human health. When investigating the characteristics of dust pollution in the working face, Zhang et al.³² investigated dust pollution characteristics in mining faces using CFD methods, analyzing the dispersion patterns of dust at the breathing zone height (1.5 m in pedestrian areas) during downwind and upwind coal cutting. Their results indicate that downwind coal cutting leads to a wider range of dust pollution at the breathing zone height. Similarly, Liu et al.³³ examined the spatiotemporal distribution of particulate matter generated by diesel vehicles under multiple operating conditions in mine roadways. Their selected sampling points were also at a height of 1.5 m. The study found that when vehicles travel downwind, the particulate concentration in the breathing zone can reach 15.79–26.32 mg/m³, with significant differences in concentration distribution between both sides of the roadway.

Research on the distribution characteristics of dust in walkway areas often focuses on variations in dust concentration and largely relies on numerical simulation methods. However, dust concentration merely provides a macroscopic reflection of coal dust exposure to workers, while some microscopic properties of coal dust, such as particle size distribution and shape factors, influence the mechanisms of dust deposition in the respiratory and pulmonary systems³⁴. Although previous studies have mentioned parameters like dust particle size, they have not specifically addressed the distribution of dust within walkway areas^{35,36}. With this premise in mind, this study focused on a fully-mechanized mining face at the Hongliulin Mine. Samples of dust at the breathing zone within walkway areas were collected during coal cutting by the shearer. In the laboratory, the samples were weighed and subjected to image analysis to investigate the distribution characteristics of coal dust within a certain range in this area, including concentration and particle size distribution. A multidimensional analysis was conducted to determine the extent of contamination by dust in this pedestrian area, providing practical recommendations for coal dust control in this mine and similar ones.

Collection of coal dust samples

Sampling location and area

The sampling location was chosen at the 15,216 mining face in Hongliulin Mine, Yulin, Shaanxi Province, with a mining height of 7 m and a mining face length of 350 m. The extraction process is fully automated and mechanized, utilizing the SL1000 shearer, with its main technical characteristics detailed in Table 1. The roof support system adopts hydraulic shields. The lithological characteristics of the coal seam are as follows: black

Parameter	Value	Parameter	Value
Mining height range (m)	3.2–6.4	Production capacity (t/h)	5000
Coal clearance height (mm)	882	Traction speed (m/min)	0–16.1
Supply voltage (V)	3300	Total machine weight (t)	173
Total installed power (kW)	2590	Machine body height (mm)	2065–2700
Drum diameter (mm)	3500	Arm swing radius (mm)	5467
Drum cutting depth (mm)	865	Undercutting depth (mm)	1005

Table 1. Main technical characteristics of the shearer.

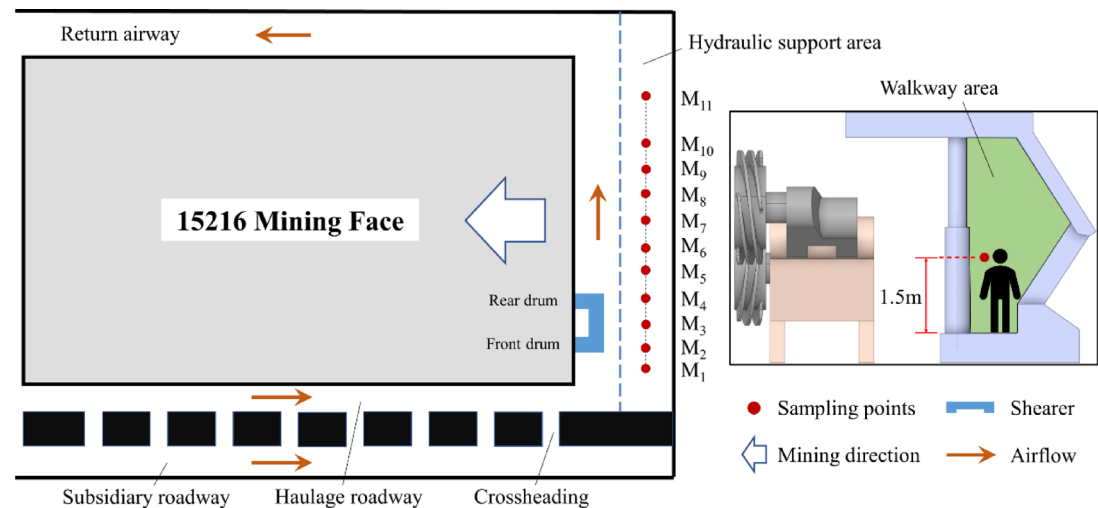


Fig. 1. Layout of the 15,216 mining face showing dust sampling spots M_1 – M_{11} along the walkway side at a height of 1.5 m with mining and airflow directions indicated.

Sampling spots	Location	Coordinate/m	Sampling spots	Location	Coordinate /m
M_1	16 m in front of the rear drum	-16	M_7	10 m behind the rear drum	10
M_2	Front drum	-10	M_8	20 m behind the rear drum	20
M_3	Middle of the shearer	-5	M_9	30 m behind the rear drum	30
M_4	Rear drum	0	M_{10}	50 m behind the rear drum	50
M_5	2 m behind the rear drum	2	M_{11}	100 m behind the rear drum	100
M_6	6 m behind the rear drum	6			

Table 2. The locations and coordinates of the sampling spots relative to the shearer.

and massive, predominantly exhibiting a semi-dull to semi-bright texture, with bands of dull coal and vitrain. The development of endogenous fractures is minimal, and the voids are filled with calcite. As shown in Fig. 1, the current system of this mining face mainly consists of the mining face roadway, haulage roadway, subsidiary roadway, and return airway. The haulage and subsidiary roadways are connected through crossheadings. Airflow enters the coal mining face from the haulage and subsidiary roadways and then exits through the return airway. Coal cutting by the shearer is the primary source of dust, and the coal dust generated during cutting moves with the airflow. Based on underground observations, during the shearer’s operation, miners observe and control the movement of the shearer and hydraulic supports in the walkway area adjacent to the supports. The primary activity areas are located approximately 10 m in front of and 20 m behind the shearer.

Given these conditions, the sampling location was set at the breathing zone height in the walkway area between the mining face supports, with a sampling height of 1.5 m³⁷, as shown in Fig. 1. A sampling spot, denoted as M_1 , was positioned in the direction against the airflow from the shearer. Three sampling spots, labeled as M_2 to M_4 , were arranged in the middle and at two drum locations on the shearer. Additionally, seven sampling spots, numbered as M_5 to M_{11} , were placed in the direction of the airflow from the shearer. Taking the rear drum M_4 of the shearer as the origin (i.e., 0 m position), the upwind direction is defined as negative and the downwind direction as positive. The shearer continuously advances while cutting coal. To ensure that all measurement points remain relatively fixed in position relative to the shearer, the measuring equipment moves forward at the same speed as the shearer during sampling. The relative positions and coordinates of all sampling spots are presented in Table 2.

Equipment information

The equipment used in this study includes the coal dust sampler and the coal dust dispersibility tester. Detailed specifications of the equipment are provided in Table 3.

Sampling method

The coal dust sampling method employed the “gravimetric method”^{30,38} and involved multiple sampling events. This sampling technique is widely adopted in the research of other scholars^{10,23}. When dusty air flows through the sampler at a fixed rate, coal dust particles deposit onto the filter membrane within the sampler, as illustrated in Fig. 2. Both before and after sampling, the filter membrane requires drying and weighing, ensuring stability during transportation. Instruments utilized throughout the process include the CCZ-20A coal dust sampler,

Information	Coal dust sampler	Coal dust dispersibility tester
Model	CCZ-20A	Rise-3022 Plus
Manufacturer	Changshu Deyu Mining Electromechanical Co., Ltd	Jinan Runzhi Technology Co., Ltd
Technical Specifications	Sampling Flow Rate: 20L/min Load Capacity: > 200 Pa Sampling Flow Rate Error: ≤ 2.5% Sampling Flow Rate Stability: ≤ 5% Flow Meter Accuracy: No less than grade 2.5 Sampling Time Error: Not exceeding 1 s within 5 min Sampling Range: Total dust or respirable dust	Measurement range: 0.1–3500 μm Microscope: Olympus CX33 Digital magnification: > 8000× Maximum resolution: 0.1 μm/pixel Repeatability error: < 1% CCD camera: ≥ 10 megapixels Automatic segmentation speed: ≤ 1 s Segmentation success rate: ≥ 99%

Table 3. Equipment information during the experimental process.

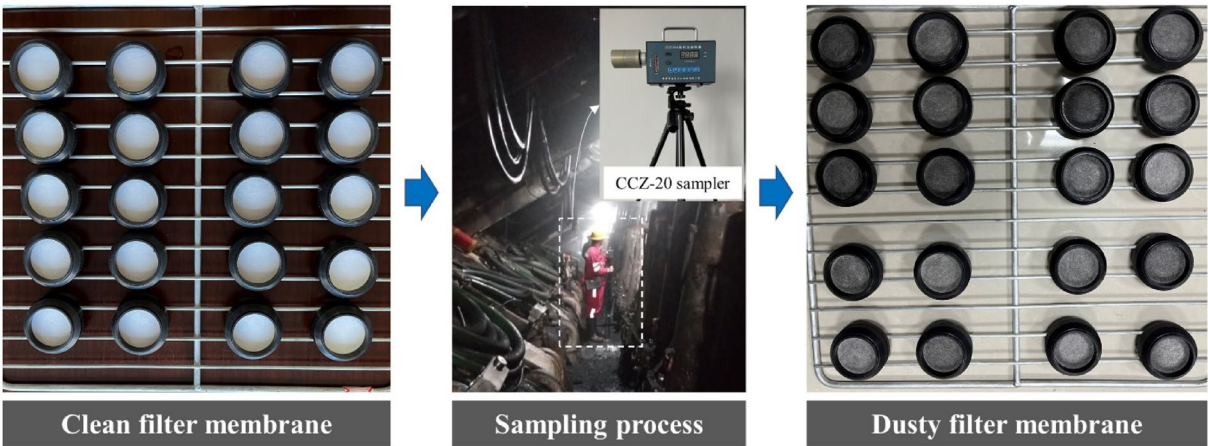


Fig. 2. Coal dust sampling from walkway area using gravimetric method showing filter membranes before and after collection.

polypropylene filter membranes, a constant temperature drying oven, and a dust-free electronic balance with an accuracy of 0.0001 mg.

Characteristic parameters of coal dust

Coal dust concentration

Coal dust mass concentration is a crucial indicator for assessing the level of coal dust pollution within a given area. It is primarily calculated based on the change in the mass of the filter membrane before and after sampling³⁸. The calculation formula is as follows:

$$c = \frac{m_2 - m_1}{V \cdot t} \times 1000 \tag{1}$$

where *c* represents the mass concentration of coal dust in the air, mg/m³; *m*₂ is the mass of the filter membrane after sampling, mg; *m*₁ is the mass of the filter membrane before sampling, mg; *V* is the sampling flow rate, L/min, with a set sampling flow rate of 20 L/min during the testing process; *t* represents the sampling duration in minutes, with a sampling duration of 3 min in this study.

Shape parameters of coal dust

The weighed dusty filter membranes are sealed for storage, preparing for the subsequent particle size analysis tests. The static image method³⁹ is chosen in this study for coal dust particle size analysis. This method not only measures particle size but also characterizes geometric parameters of the particles. The particle size analysis employs the Rise-3022 plus coal dust dispersibility tester (10 × magnification), conforming to industry standards⁴⁰, with an anhydrous ethanol dispersant. The primary measurement steps are depicted in Fig. 3. Examples of observed coal dust particle shapes are illustrated in Fig. 4.

Due to the irregular shape of particles, the study of coal dust particle shape characteristics primarily considers parameters such as equivalent circle diameter, aspect ratio, and circularity. The images in Fig. 4 were analyzed using the built-in software of the Rise-3022 plus coal dust dispersibility tester. The main characteristic parameters are shown in Fig. 5.

(1) Equivalent circle diameter

Equivalent circle diameter refers to the diameter of a circle with the same projected area as the particle.

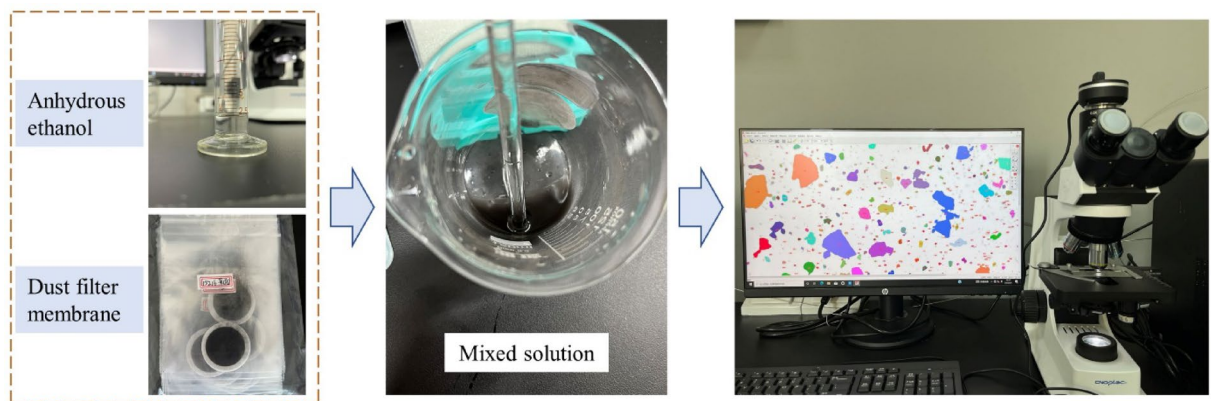


Fig. 3. Dust particle size test procedure showing ethanol and filter membrane preparation solution mixing and particle size analysis.

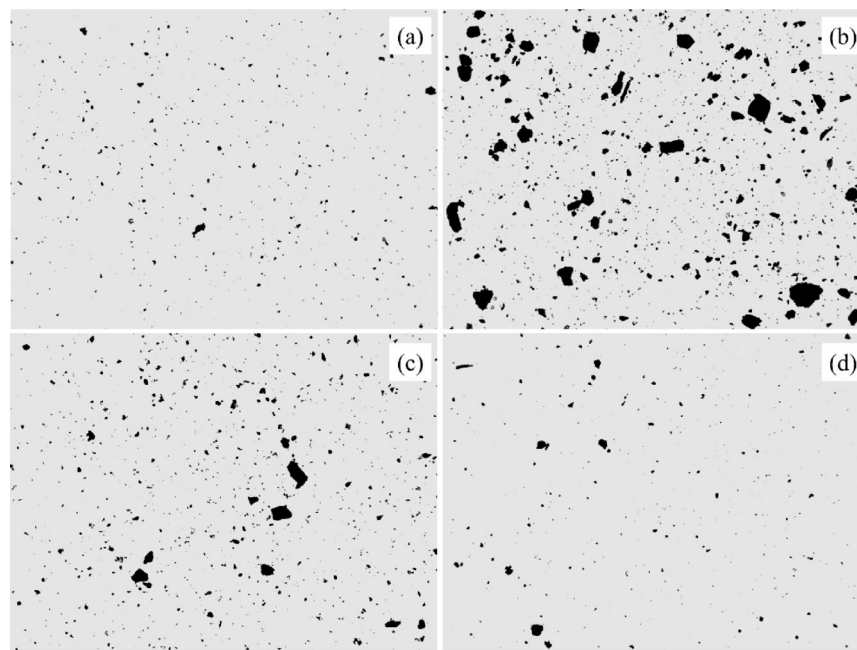


Fig. 4. Microscopic images of dust particles collected from different sampling locations M_1 , M_4 , M_6 , and M_9 . (a) M_1 (-16 m); (b) M_4 (0 m); (c) M_6 (10 m); (d) M_9 (50 m).

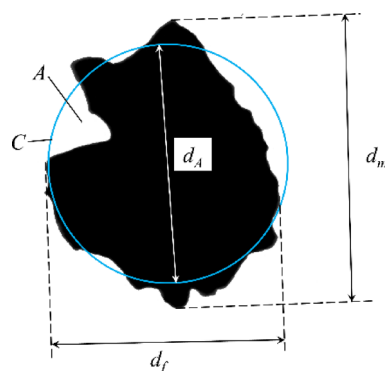


Fig. 5. Shape characteristics of dust particles showing key dimensional features.

$$d_c = \sqrt{\frac{4A}{\pi}} \quad (2)$$

where d_c represents the equivalent circle diameter, μm ; and A is the projected area of the particle, μm^2 .

(2) Aspect ratio

Aspect ratio is a parameter that characterizes particle shape and can be used to assess the shape of a particle. The closer the aspect ratio is to 100%, the closer the particle's length and width are; the smaller the aspect ratio, the more elongated the particle's shape.

$$E = \frac{d_f}{d_m} \times 100\% \quad (3)$$

where E represents the aspect ratio, %; d_m is the Feret length, which is the maximum distance between parallel lines along the particle contour in micrometers, μm ; and d_f is the distance between parallel lines perpendicular to d_m , μm .

(3) Circularity

Circularity represents the degree to which the particle (or its projected area) is similar to a circle, taking into account the smoothness of the perimeter⁴¹.

$$C = \sqrt{\frac{4\pi A}{p^2}} \quad (4)$$

where C represents circularity, and p represents the actual perimeter of the particle, m.

Results and discussion

Concentration distribution of coal dust

Figure 6 visually presents the distribution of coal dust concentrations at various sampling points along the coal mining face. The data shows that the highest coal dust concentration, reaching 283 mg/m^3 , is observed at the rear drum of the coal cutter at M_4 , forming the peak dust emission zone. In contrast, the sampling point M_1 (located at -16 m , farthest from the windward side of M_4) has the lowest dust concentration, only 10 mg/m^3 , reflecting the significant impact of airflow direction on dust dispersion. Although M_{10} is farther from the dust source, its dust concentration reaches 47 mg/m^3 due to its position on the leeward side, where airflow continuously carries and accumulates dust particles in this area, resulting in a higher concentration than at M_1 . Along the airflow direction, from the front drum of the coal cutter to the rear drum, the coal dust concentration gradually increases, rising from 49 mg/m^3 to 283 mg/m^3 . This peak indicates the direct impact of the cutting process on dust emissions. As shown in Fig. 6, the coal dust concentration at M_5 is 52 mg/m^3 , indicating an 81.6% reduction in dust concentration in the pedestrian area of the hydraulic support within 50 m from the second cutting drum.

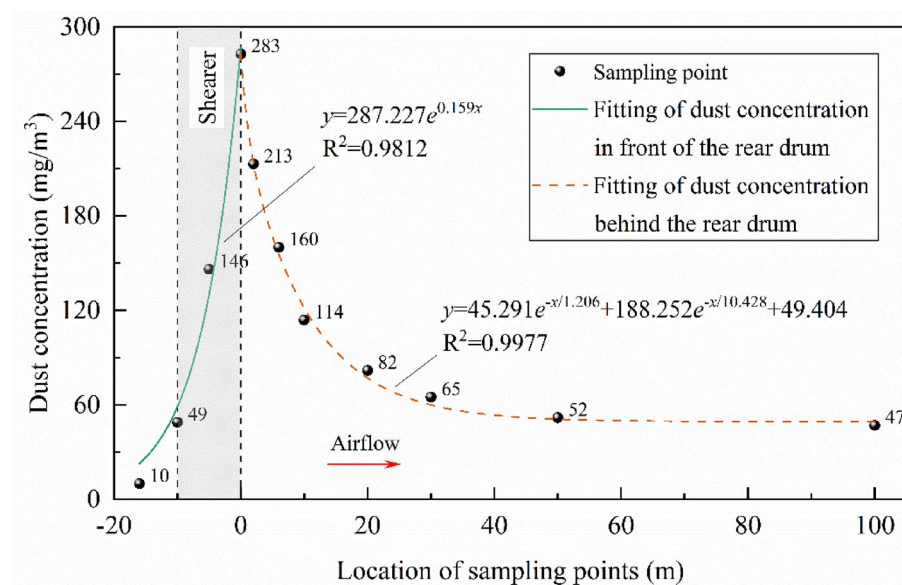


Fig. 6. Variation characteristics of dust concentration in the walkway area showing fitted curves for dust levels in front of and behind the rear drum.

Subsequently, the dust concentration shows a slow declining trend, with a decrease of only 5 mg/m^3 between 50 and 100 m. Therefore, it can be inferred that beyond the measurement range, the dust concentration reduction rate further slows down and tends to stabilize.

Figure 6 displays the coal dust concentration values at various measurement points on the mining face. The data reveals that the coal dust concentration at the rear drum, M_4 , of the shearer is the highest within the entire measurement range, measuring 283 mg/m^3 . At sampling point M_1 , situated at the furthest point downstream of M_4 (with coordinates at -16 m), the coal dust concentration within the breathing zone of workers is merely 10 mg/m^3 , representing the lowest concentration across the entire measurement range. Following the airflow direction from the front drum of the shearer to the rear drum, the dust concentration escalates from 49 mg/m^3 to 283 mg/m^3 , constituting the maximum coal dust concentration among all measurement points. As depicted in Fig. 6, the coal dust concentration at M_{10} is recorded at 52 mg/m^3 , indicating an 81.6% reduction in coal dust concentration within a 50 m range downstream of the second cutting drum, in the vicinity of hydraulic support walkway area. Subsequently, the dust concentration gradually diminishes within the measurement range beyond M_{10} , reaching 47 mg/m^3 at a distance of 100 m. This suggests that coal dust concentration is expected to remain relatively stable beyond the measurement range, decreasing at a slow rate.

The coal dust in the walkway area originates from the mining face and is minimally influenced by other factors. The coal dust concentration exhibits a gradual decrease with increasing distance. To more clearly reveal the variation in coal dust concentration with distance from the shearer, a quantitative analysis was conducted on the coal dust concentration distribution at the hydraulic support area of the coal mining face. Since the dust in this region mainly originates from the coal mining process and is minimally affected by other disturbances, it can be assumed that the concentration variation is primarily influenced by the relative distance to the shearer. Taking the distance from the shearer's rear drum as the independent variable x and the measured coal dust concentration as the dependent variable y , multiple regression fittings were performed using different functional forms. The results show that the power function model provides a good fit in the area ahead of the shearer, with the corresponding regression equation:

$$y = 287.227e^{0.159x} \quad (5)$$

For the area behind the shearer, a double exponential decay function was used for fitting, which demonstrated superior performance compared to other forms. The expression is:

$$y = 45.291e^{-x/1.206} + 188.252e^{-x/10.428} + 49.404 \quad (6)$$

The model performance evaluation results indicate that the correlation coefficient R^2 for Eq. is 0.9812, while that for Eq. is 0.9977. These high fitting accuracies suggest that the models effectively capture the actual trend of coal dust concentration variation with distance. This further confirms a significant negative correlation between coal dust concentration and distance from the shearer, with distinct decay characteristics in different regions.

After coal fragmentation, various sizes of coal dust particles are formed. These particles have an initial velocity, it can be inferred that larger particles will experience greater acceleration in the vertical direction, leading to faster settling. Therefore, large-sized coal dust particles settle rapidly on the downwind side of the shearer, explaining the phenomenon of a rapid decrease in coal dust concentration within 20 m behind the shearer's rear drum. Furthermore, due to the relatively stable nature of the airflow field, once the larger-sized coal dust particles have settled, smaller-sized particles tend to linger in the airflow for a longer time. This results in a gradual reduction in coal dust concentration between 20 and 100 m downstream.

Variations in coal dust quantity at different spots

To study the variation patterns of coal dust quantities, Fig. 7 presents the relative change rates of total dust ε_t , respirable dust ε_r , and non-respirable dust ε_{nr} at different locations, with the coal dust quantity at the rear drum M_4 of the shearer as the reference. The relative change rates of the three types of coal dust at location M_5 are all 1.12, the highest among all measurement points. This indicates that M_5 has the highest total, respirable, and non-respirable dust quantities among all locations. For the upwind side of the shearer's rear drum, location M_1 has the lowest relative change rate ε_t of total dust quantity, indicating the least amount of coal dust. The lowest relative change rates for total, respirable, and non-respirable dust are 0.43 (M_1), 0.4 (M_1), and 0.15 (M_2), respectively. On the other hand, for the downwind side of the shearer's rear drum, location M_{11} has the lowest relative change rate ε_t of total dust quantity, indicating the least amount of coal dust. The lowest relative change rates for total, respirable, and non-respirable dust are 0.33 (M_{11}), 0.37 (M_{11}), and 0.04 (M_{11}), respectively.

It can be observed that the trends in the quantity changes of the three types of coal dust are consistent. Specifically, there is a sharp decrease in coal dust quantity in the intervals M_4 - M_3 and M_5 - M_8 , a slow decrease in the intervals M_3 - M_1 and M_8 - M_{11} , and a slight increase in coal dust quantity in the M_4 - M_5 interval. Among the 11 measurement points, except for M_4 and M_5 where $\varepsilon_r = \varepsilon_t = \varepsilon_{nr}$, the coal dust quantity change rates at other locations follow the pattern $\varepsilon_r > \varepsilon_t > \varepsilon_{nr}$. This indicates that within the measurement range, non-respirable coal dust quantities decrease more rapidly, suggesting that the settling rate of non-respirable particles ($d_p > 10 \mu\text{m}$) at the height of the breathing zone is significantly higher than that of respirable particles ($d_p \leq 10 \mu\text{m}$).

Particle size distribution characteristics of coal dust

The particle size distribution of coal dust on the coal mining face is a crucial indicator for assessing the extent of coal dust hazards. Unlike mass distribution or volume distribution, this study focuses on the quantity distribution of particles of different sizes within the coal dust generated during the coal mining process, which

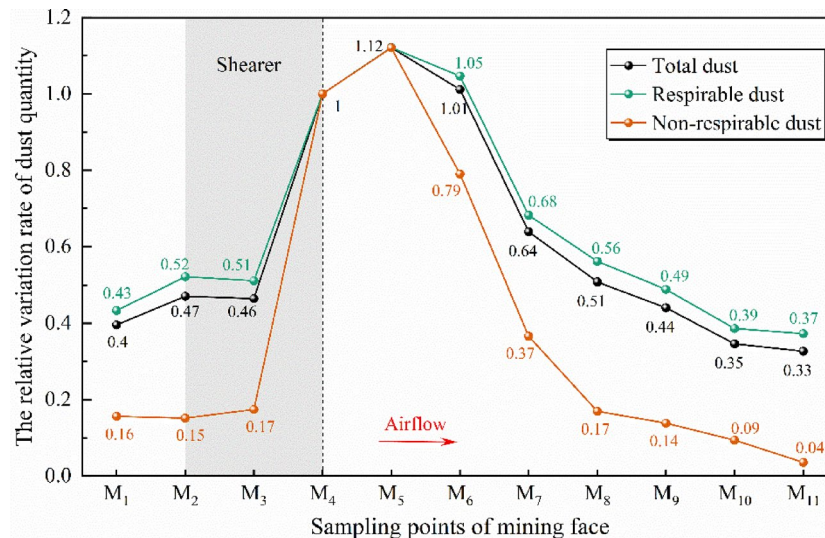


Fig. 7. Relative change rate of dust quantity at different sampling locations based on M_4 .

provides a more intuitive representation of dust pollution. The following sections investigate the relative quantity distribution, cumulative quantity distribution, and characteristic particle size distribution of coal dust. In Fig. 4, it can be observed that the actual shape of coal dust is not spherical but irregular. Therefore, we use the equivalent surface diameter d_c to represent the particle diameter d_p . The formulas for calculating the relative quantity distribution f_i and cumulative quantity distribution F_i of coal dust are as follows:

$$\begin{cases} f_i = \frac{n_i}{\sum_{j=1}^N n_j} \times 100\% \\ F_i = \frac{\sum_{j=1}^i n_j}{\sum_{j=1}^N n_j} \times 100\% \end{cases} \quad (7)$$

where f_i is the relative quantity distribution of particles in the i th particle size interval, %; F_i is the cumulative quantity distribution of particles, %; n_i is the number of particles in the i th particle size interval. The relative quantity distribution and cumulative quantity distribution of coal dust are illustrated in Fig. 8.

The particle size distribution in Fig. 8 reveals that the largest coal dust particle size does not exceed 100 μm . It further divides the particles into six size intervals: 0–5 μm , 5–10 μm , 10–20 μm , 20–50 μm , and 50–100 μm . The percentage of coal dust in each particle size interval is shown in Table 4. From the data in the table, it is evident that, across all sampling points, as the particle size interval increases, the quantity of coal dust gradually decreases. Specifically, the highest proportion of coal dust is in the 0–5 μm size range, while the lowest proportion is in the 50–100 μm range. Coal dust particle sizes are primarily distributed between 0–50 μm , with the majority falling within the 0–10 μm range. This indicates that the overall variation in total dust quantities, as shown in Fig. 7, is primarily influenced by changes in respirable dust quantities. Regarding respirable coal dust particles (0–10 μm), the proportion of 0–5 μm coal dust exceeds 60% at all points, with the highest value at 73.7% (M_{11}) and the lowest at 60.7% (M_4). For the 5–10 μm range, the proportion exceeds 20%, with the highest at 35% (M_{10}) and the lowest at 21.8% (M_7). In the case of non-respirable coal dust particles (10–100 μm), the proportion of 10–20 μm coal dust does not exceed 10%, with the highest at 9.8% (M_4) and the lowest at 1.5% (M_{11}). For the 20–50 μm range, the proportion does not exceed 4%, with the highest at 3.9% (M_5) and the lowest at 0% (M_{11}). Finally, the 50–100 μm coal dust is only present at M_4 and M_6 , with proportions of 0.24% in both cases. The data in Table 4 also indicate that as the distance from the rear drum of the coal shearer increases, the percentage variation of non-respirable particles within the same interval decreases. In other words, the quantity variation of respirable dust is lower than that of non-respirable dust.

Figure 9 displays the characteristic particle size distribution of coal dust, where D5, D10, D30, D50, D60, D90, and D97 represent the characteristic particle sizes when cumulative percentages of coal dust reach 5%, 10%, 30%, 50%, 60%, 90%, and 97%, respectively. Firstly, the values of D5, D10, D30, D50, and D60 are very similar across all measurement points, and their particle sizes are all less than 5 μm . This indicates the presence of a significant number of tiny particles at these measurement points. Additionally, the parameter D97 exhibits consistently high values across all measurement points, suggesting the presence of exceptionally large particles in these areas. In particular, at points M_4 and M_5 , the D97 values are 21.9 μm and 23.44 μm , significantly higher than the other measurement points, indicating the existence of unusually large coal dust particles in that region, consistent with the particle size images in Fig. 4. Except for these two locations, the D97 values at other measurement points range from approximately 8.9 μm to 15.5 μm .

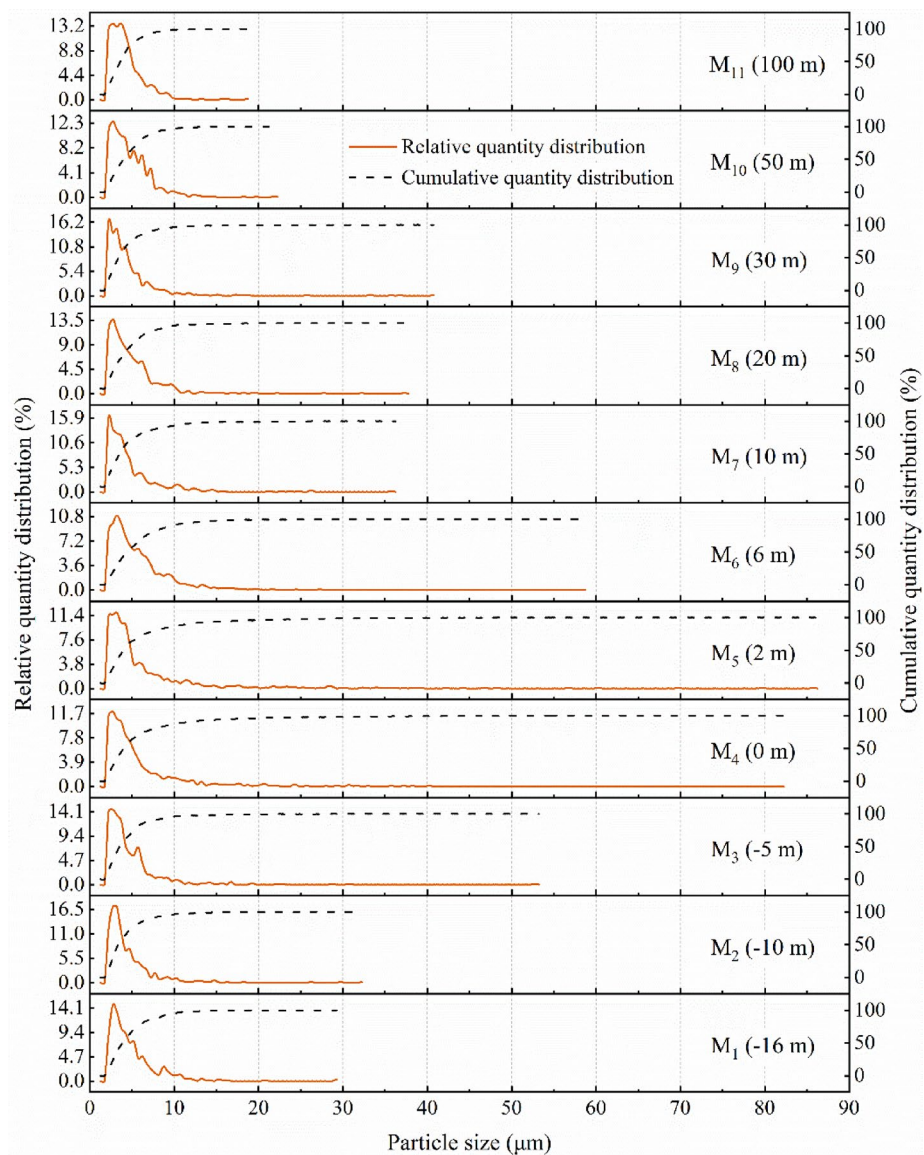


Fig. 8. Relative quantity and cumulative quantity distribution of coal dust at different sampling heights.

Sampling spots	Particle size ranges (μm)				
	0–5	5–10	10–20	20–50	50–100
M ₁	63.64%	30.97%	4.93%	0.46%	0.00%
M ₂	72.15%	23.45%	4.02%	0.39%	0.00%
M ₃	67.85%	27.03%	4.46%	0.66%	0.00%
M ₄	60.30%	26.04%	9.82%	3.60%	0.24%
M ₅	62.10%	24.25%	9.79%	3.86%	0.00%
M ₆	60.70%	28.63%	9.22%	1.21%	0.24%
M ₇	70.42%	21.76%	6.49%	1.34%	0.00%
M ₈	62.79%	32.65%	4.08%	0.48%	0.00%
M ₉	73.03%	22.68%	3.60%	0.69%	0.00%
M ₁₀	61.27%	35.04%	3.52%	0.18%	0.00%
M ₁₁	73.69%	24.81%	1.49%	0.00%	0.00%

Table 4. Percentage of dust quantity in different particle size ranges.

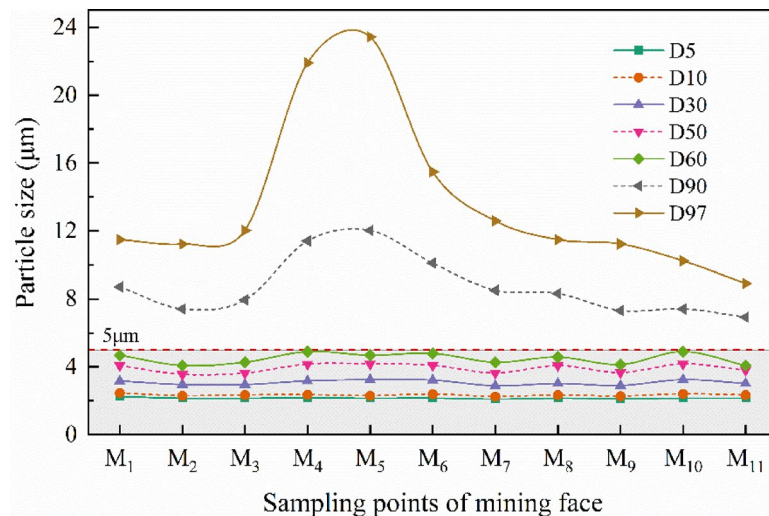


Fig. 9. Characteristic particle size of dust in different regions of the mining face showing variations across sampling locations.

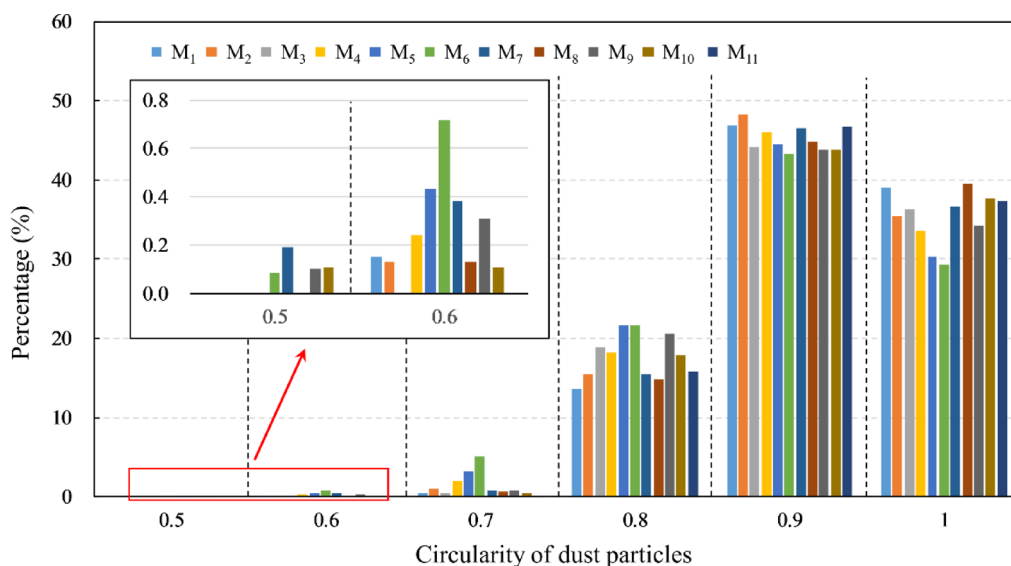


Fig. 10. Distribution of dust particle circularity showing percentage variations across different sampling locations.

Shape characteristics of coal dust

Circularity characteristics

The circularity of coal dust particles was divided into six intervals: 0–0.5, 0.5–0.6, 0.6–0.7, 0.7–0.8, 0.8–0.9, and 0.9–1.0. Figure 10 illustrates the distribution characteristics of coal dust circularity across 11 different sampling locations. The results show that particles with circularity between 0.8 and 0.9 accounted for the highest proportion, exceeding 40% of the total. Particles with circularity values between 0.9 and 1.0 also represented a significant proportion, generally ranging from 29 to 40%. For additional context, a circularity value closer to 1.0 indicates a particle is more spherical, while lower values suggest more irregular or elongated shapes. The dominance of particles in the 0.8–0.9 interval indicates that most coal dust particles are relatively compact rather than highly elongated or irregular. In contrast, particles with circularity between 0.7 and 0.8 accounted for 13% to 22%, and those with circularity below 0.7 contributed less than 5%. This distribution pattern suggests that coal dust particles at a height of 1.5 m in the support area exhibit relatively high circularity, implying a more symmetrical morphology compared to particles with lower circularity. Moreover, the distribution of circularity remained relatively stable across different sampling locations, indicating that spatial variation had a limited impact on particle circularity.

Aspect ratio characteristics

Figure 11 presents the variation in aspect ratio of coal dust particles across different locations. The aspect ratio reflects the degree of particle elongation, where a value approaching 1 indicates a more spherical shape, while lower values suggest a more elongated or needle-like morphology. The results reveal that more than 15% of the coal dust particles had an aspect ratio close to 1, indicating that a considerable proportion of particles were nearly spherical. At locations M_5 and M_6 , the aspect ratio of coal dust particles ranged from 0.1 to 1, while at location M_4 , it ranged from 0.2 to 1. At other locations, the aspect ratios were mostly distributed between 0.3 and 1. At locations M_4 , M_5 , and M_6 , the aspect ratios were relatively uniformly distributed between 0.5 and 1, whereas greater fluctuations were observed at other locations. Notably, the proportion of particles with aspect ratios between 0.9 and 1 increased beyond location M_7 . Overall, it can be inferred that the aspect ratio of coal dust particles is more uniformly distributed in the regions behind the shearer's rear drum and on the leeward side (M_4 to M_6), while at other locations, aspect ratios tend to be larger. In addition, this pattern suggests that in the vicinity of hydraulic supports, more elongated coal dust particles are more likely to settle from the airflow, thereby influencing the spatial distribution of particle morphology.

Discussion

Based on the on-site investigation, it is evident that, apart from the essential ventilation and dust removal measures, the 15,216 mining face primarily employs internal and external spraying within the shearer for dust suppression. However, research results indicate that under the existing dust control measures, the coal dust mass concentration levels in the walkway area's breathing zone of this large mining height coal seam during excavation remain remarkably high. The highest concentration recorded can reach up to 284 mg/m^3 , and even at a distance of 16 m upwind from the front drum (in the direction against the airflow), coal dust concentrations still reach 10 mg/m^3 . These concentrations significantly exceed the regulatory limits^{8,9}. Taking the prescribed total dust limit concentration of 4 mg/m^3 as a reference, the measured dust concentrations in the sampling range are 400% to 7100% of the regulatory value. This underscores the substantial dust generation during coal fragmentation by the shearer and the limitations of the current spray dust control measures. Regarding particle shape characteristics, the coal dust exhibits a limited range of circularity, but the circularity of coal dust at all locations is relatively high. On the other hand, the aspect ratio of coal dust particles has a wide and evenly distributed range. This suggests that the coal dust particles on this working face have relatively smooth surfaces but are elongated, primarily taking on an elongated, ribbon-like form.

Due to the unavoidable harm inflicted on the human lungs by respirable coal dust, the research findings allow for further classification of the distribution of respirable dust in different regions, as illustrated in Fig. 12. In the walkway zone, regions with a respirable dust quantity change rate $\varepsilon_r > 1$ are situated at 0 to 6 m, regions with $0.5 < \varepsilon_r \leq 1$ are found at -10 to 0 m and 6 to 30 m, while in other regions, $0 < \varepsilon_r \leq 0.5$. It is evident that the closer one is to the dust source of the shearer, the higher the quantity of respirable dust, indicating greater harm to human health. During coal-cutting by the shearer, miners are required to closely observe and remotely control the shearer, hydraulic supports, and other equipment in the walkway area. During this time, they must spend

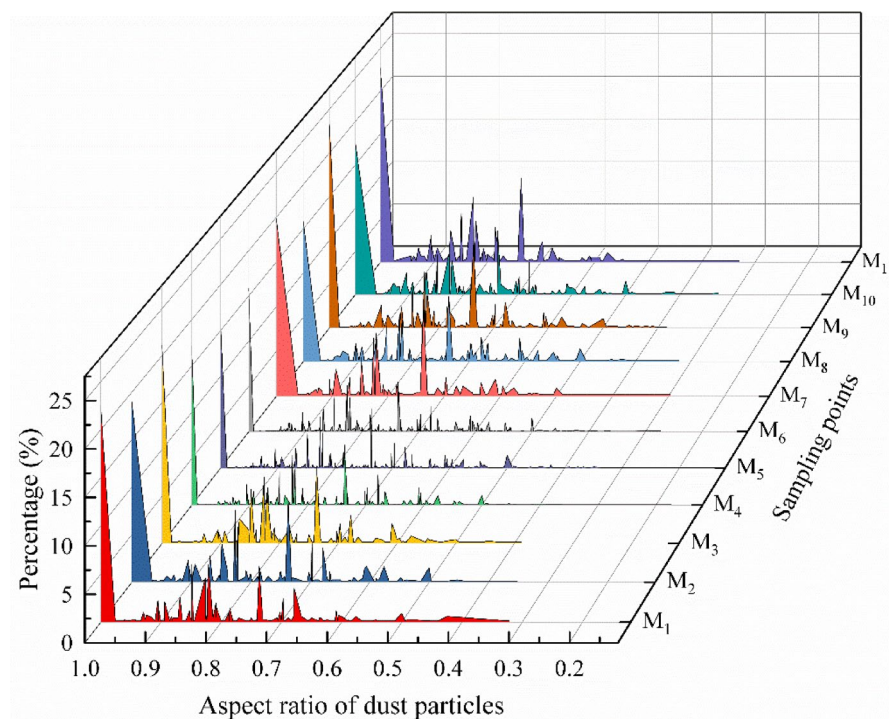


Fig. 11. Distribution of dust particle aspect ratio showing variations across different sampling locations.

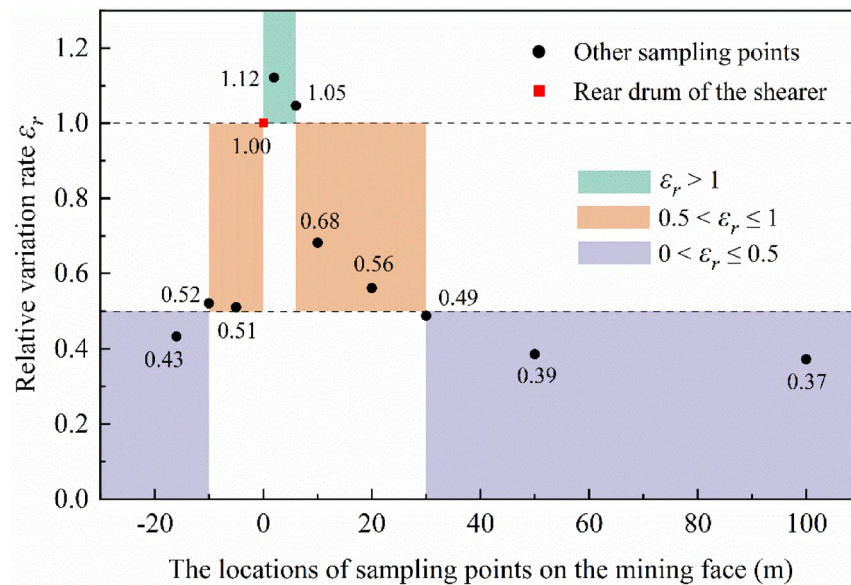


Fig. 12. Relative variation rate of respirable dust quantity at different sampling locations based on M_4 .

extended periods in areas with $\epsilon_r > 1$ and $0.5 < \epsilon_r \leq 1$. Consequently, they inhale a larger amount of respirable coal dust, which can lead to greater damage to their lungs over time. Therefore, in these two regions with $\epsilon_r > 1$ and $0.5 < \epsilon_r \leq 1$, the walkway area corresponding to the shearer's operating area and its downwind side of 30 m, more effective dust reduction measures are imperative, especially the application of technologies and equipment to reduce respirable dust.

The coal dust samples in this study were obtained from the Hongliulin Mine in the northern Shaanxi mining area. The research results have shed light on the current status of coal dust pollution on the mining face. However, the revealed characteristics of coal dust distribution have significant implications for both dust control and dust dispersion research in the Hongliulin Mine and similar high mining height working faces. Specifically, this value is reflected in several aspects. First, current dust control technologies tend to focus on capturing or settling dust near the source. The latest systematic review by NIOSH has summarized dust control techniques for coal mining faces³⁰, which can be further refined and applied to dust management in pedestrian zones. Second, coal dust mitigation should implement precise control measures across different particle size ranges, focusing on variations in dust particle counts rather than solely targeting concentration reduction. In particular, it is essential to enhance the control of coal dust particles smaller than 10 μm by employing high-efficiency water mist dust suppression technology, a "long extraction–short pressure" ventilation strategy, and novel dust suppression materials and additives. Finally, the shape parameters of coal dust particles should be considered as key influencing factors in dust control research, especially in computational simulations and spray dust suppression studies. Currently, most CFD studies simplify by assuming coal dust particles to be ideal spheres, thus neglecting the impact of actual particle morphology on dispersion and settling behavior^{11,24,32}.

Conclusions

In this study, coal dust samples were collected from the breathing zone of the pedestrian walkway in the mining face to analyze in detail the distribution of dust at various locations during the operation of the shearer. The main conclusions are as follows: Even with dust suppression measures implemented in the walkway region, dust pollution remains severe, with concentrations far exceeding the 4 mg/m^3 limit stipulated by the Coal Mine Safety Regulations. Specifically, the highest dust concentration was recorded at the location corresponding to the rear drum of the shearer, reaching up to 284 mg/m^3 , while the lowest concentration, only 16 mg/m^3 , was observed 16 m in front of the shearer. This phenomenon is attributed to the combined effects of the airflow field and the gravitational settling of coarse dust particles, which result in a rapid decline in dust concentration within 50 m behind the shearer, whereas fine particles, due to their suspension and transport within the airflow, maintain relatively stable concentrations beyond this distance. Furthermore, variations in dust concentration across different positions do not directly correspond with changes in the number of dust particles. The greatest particle count was observed approximately 6 m behind the shearer, and the rate of change in the number of non-respirable dust particles was higher than that of respirable dust, indicating that coarse particles settle more quickly. Moreover, the distribution of respirable dust particle counts can be categorized into three distinct regions, with workers predominantly located in the two regions exhibiting relatively high respirable dust concentrations. Additional analysis of particle size distribution reveals that as particle size decreases, its relative frequency increases. At all sampling points, particles in the 0–5 μm range account for over 60% of the total, and apart from the region directly corresponding to the shearer, particles in the 0–10 μm range exceed 90%. In addition, the roundness of the dust particles in the pedestrian area is relatively concentrated and overall high, whereas the distribution of the aspect ratio is broad and quite uniform, suggesting that while the particle surfaces

are relatively smooth, their shapes tend to be elongated and rod-like. These results indicate that effective dust control measures in high-extraction mining faces remain lacking—especially in the pedestrian areas—resulting in a situation where the intensity of coal extraction is high, yet dust mitigation efforts are insufficient. This discrepancy calls for increased attention and the deployment of more advanced technological equipment for dust control in the pedestrian zones, with an emphasis on reducing the number of respirable dust particles.

Although this study offers valuable insights for the precise management of dust and advances research in related fields, certain limitations remain. For example, the study is based solely on data from a single fully mechanized mining face, which limits sample representativeness and the comprehensiveness of the sampling point distribution. Moreover, the research primarily focuses on short-term data and lacks long-term continuous monitoring, while the continuous movement of the shearer during sampling may introduce certain measurement errors. Future research should address these shortcomings and further explore the relationship between dust exposure duration and health risks from an occupational health perspective.

Data availability

The data and figures analyzed during the current study are available from the corresponding author upon reasonable request.

Received: 23 December 2024; Accepted: 14 May 2025

Published online: 19 May 2025

References

1. Srikanth, R. *Coal characteristics and respirable dust generation*. The Pennsylvania State University (1997).
2. Kundu, S. K., Zanganeh, J., Eschebach, D. & Moghtaderi, B. Explosion severity of methane–coal dust hybrid mixtures in a ducted spherical vessel. *Powder Technol.* **323**, 95–102 (2018).
3. Chen, G. et al. Statistical analysis on dust explosion accidents in China from 2005 to 2020. *China Saf. Sci. J.* **32**, 76–83 (2022).
4. Sapko, M. J., Cashdollar, K. L. & Green, G. M. Coal dust particle size survey of US mines. *J. Loss Prev. Process Ind.* **20**, 616–620 (2007).
5. Bell, J. L. Trends in pneumoconiosis deaths—United States, 1999–2018. *MMWR Morb. Mortal. Wkly. Rep.* **69**, 693 (2020).
6. XINHUANET. Occupational pneumoconiosis incidence has decreased by over 50% in the past decade, effectively controlling the prevalence of key occupational diseases. <http://www.news.cn/2022-04/28/c_1128602800.htm (2022).
7. National Health Commission of the People's Republic of China. *Statistical Bulletin on the Development of China's Health and Medical Care in 2021*. <http://www.nhc.gov.cn/guihuaxxs/s3586s/202207/51b55216c2154332a660157abf28b09d.shtml> (2022).
8. Ministry of Emergency Management of the People's Republic of China & National Mine Safety Administration. *Safety Regulations in Coal Mine* (Emergency Management Press, 2022).
9. Li, W. & Zhu, Q. Comparison and analysis research on occupational exposure limits of coal dust between China and foreign countries. *Chin. J. Ind. Hygiene Occup. Dis.* **42**, 107–111 (2024).
10. Zhang, G. et al. Numerical simulation and engineering application of multistage atomization dustfall at a fully mechanized excavation face. *Tunn. Undergr. Space Technol.* **104**, 103540 (2020).
11. Zhou, G., Zhang, Q., Bai, R., Fan, T. & Wang, G. The diffusion behavior law of respirable dust at fully mechanized caving face in coal mine: CFD numerical simulation and engineering application. *Process Saf. Environ.* **106**, 117–128 (2017).
12. Yuan, L. Scientific conception of coal mine dust control and occupational safety. *J. China Coal Soc.* **45**, 1–7 (2020).
13. Zuo, Q. *Experimental study on the characteristic of coal dust explosion and the explosion suppression technology*. Shandong University of Science and Technology (2010).
14. Nie, B., Li, X., Yang, T., Hu, W. & Guo, J. Distribution of PM_{2.5} dust during mining operation in coal workplace. *J. China Coal Soc.* **38**, 33–37 (2013).
15. Guo, W. On-site measurement study on distrition pattern of dust concentration in Lingquan mine. *J. Saf. Sci. Technol.* **7**, 65–68 (2011).
16. Tan, C., Jiang, Z., Wang, M. & Chen, Y. Similarity experiment on multi-source dust diffusion law in fully mechanized caving face. *J. China Coal Soc.* **40**, 122–127 (2015).
17. Jiang, Z., Yapeng, W. & Jiuzhu, W. Studies on dust pollution induced by high-ore pass unloading airflow. *J. Hunan Univ. Nat. Sci.* **46**, 114–123 (2019).
18. Reed, W. *Significant Dust Dispersion Models for Mining Operations*, Vol. 9478 (Department of Health and Human Services, Centers for Disease Control and Prevention (NIOSH), 2005).
19. Bhaskar, R. *Spatial and temporal behavior of dust in mines—theoretical and experimental studies*. The Pennsylvania State University (1987).
20. Vora, J. *Dust Dispersion Modeling For Opencast Mines*. National Institute of Technology (2010).
21. Ndunguma, D. D. *Computational Fluid Dynamics model for controlling dust and methane in underground coalmines*. University of Pretoria (2011).
22. Sullivan, P. & Heerden, J. V. The simulation of environmental conditions in continuous miner developments using computational fluid dynamics. *J. Mine Vent. Soc. S. Afr.* **46**, 2–11 (1993).
23. Liu, Q. et al. Research on tunnel ventilation systems: Dust Diffusion and Pollution Behaviour by air curtains based on CFD technology and field measurement. *Build. Environ.* **147**, 444–460 (2019).
24. Du, T. et al. CFD modeling of coal dust migration in an 8.8-meter-high fully mechanized mining face. *Energy* **212**, 118616 (2020).
25. Torano, J., Torno, S., Menendez, M. & Gent, M. Auxiliary ventilation in mining roadways driven with roadheaders: Validated CFD modelling of dust behaviour. *Tunn. Undergr. Space Technol.* **26**, 201–210 (2011).
26. Yuez, L., Saad, A., Agus, S. P. & Jundika, K. C. Prediction of air flow, methane, and coal dust dispersion in a room and pillar mining face. *Int. J. Min. Sci. Technol.* **27**, 657–662 (2017).
27. Chen, L., Ma, Y., Ghaleb, M. & Liu, G. Study on dust pollution law and ventilation optimization of roadway excavation and shotcrete simultaneous operation. *J. Clean Prod.* **379**, 134744 (2022).
28. Zhang, W., Xue, S., Tu, Q., Shi, G. & Zhu, Y. Study on the distribution characteristics of dust with different particle sizes under forced ventilation in a heading face. *Powder Technol.* **406**, 117504 (2022).
29. National Institute for Occupational Safety and Health. *Hierarchy of controls*. <https://www.cdc.gov/niosh/topics/hierarchy/default.html> (2015).
30. Colinet, J., Halldin, C. N. & Schall, J. *Best practices for dust control in coal mining* (2021).
31. Das, A. et al. Size fraction of hazardous particulate matter governing the respiratory deposition and inhalation risk in the highly polluted city Delhi. *Environ. Sci. Pollut. Res.* **30**, 11600–11616 (2023).

32. Zhang, G., Zhou, G., Song, S., Zhang, L. & Sun, B. CFD investigation on dust dispersion pollution of down/upwind coal cutting and relevant countermeasures for spraying dustfall in fully mechanized mining face. *Adv. Powder Technol.* **31**, 3177–3190 (2020).
33. Liu, C. et al. Numerical study on temporal and spatial distribution of particulate matter under multi-vehicle working conditions. *Sci. Total Environ.* **862**, 160710 (2023).
34. World Health Organization. *Determination of airborne fibre number concentrations: A recommended method, by phase-contrast optical microscopy (membrane filter method)* (World Health Organization, 1997).
35. Assemi, S., Pan, L., Wang, X., Akinseye, T. & Miller, J. D. Size distribution, elemental composition and morphology of nanoparticles separated from respirable coal mine dust. *Minerals* **13**, 97 (2023).
36. Pang, J. et al. Study on dust distribution features of fully-mechanized heading face under long distance exhausted and short distance forced ventilation. *Coal Sci. Technol.* **45**, 76–81 (2017).
37. Ministry of Coal Industry of the People's Republic of China. Methods for measuring dust concentration and dispersity. MT 79-84 (1984).
38. Standardization Administration. Ambient air-Determination of particulate matter mass concentration-Gravimetric method. GB/T 39193-2020 (2020).
39. Yang, Y., Wei, Z., Chen, Y. & Ren, B. Study on the shapes of tailings particles based on microscopy and image processing technologies. *Chin. J. Rock Mech. Eng.* **36**, 3689–3695 (2017).
40. National Health Commission of the People's Republic of China. Determination of dust in the air of workplace-Part 3: Distribution of particulate. GBZ/T 192.3-2007 (2007).
41. International Organization for Standardization. Representation of results of particle size analysis—Part 6: Descriptive and quantitative representation of particle shape and morphology. ISO 9276-6:2008 (2008).

Acknowledgements

This study was supported by the Open Research Fund of the Joint National-Local Engineering Research Centre for Safe and Precise Coal Mining (Anhui University of Science and Technology) (No. EC2022019) during the experimental process and the Daily Financial Support For Postdoctoral Researchers in Guizhou Province during the manuscript revision process.

Author contributions

W.Z. wrote the original manuscript. Q.T. conceived the experiment. Q.T. and S.X. conducted the formal review and editing. W.Z. and Z.Z. performed the experiments. F.X. and X.X. conducted the statistical analysis and generated the figures. C.L. was responsible for sample collection and processing. All authors reviewed the manuscript.

Declarations

Competing interests

The authors declare no competing interests.

Additional information

Correspondence and requests for materials should be addressed to Q.T.

Reprints and permissions information is available at www.nature.com/reprints.

Publisher's note Springer Nature remains neutral with regard to jurisdictional claims in published maps and institutional affiliations.

Open Access This article is licensed under a Creative Commons Attribution-NonCommercial-NoDerivatives 4.0 International License, which permits any non-commercial use, sharing, distribution and reproduction in any medium or format, as long as you give appropriate credit to the original author(s) and the source, provide a link to the Creative Commons licence, and indicate if you modified the licensed material. You do not have permission under this licence to share adapted material derived from this article or parts of it. The images or other third party material in this article are included in the article's Creative Commons licence, unless indicated otherwise in a credit line to the material. If material is not included in the article's Creative Commons licence and your intended use is not permitted by statutory regulation or exceeds the permitted use, you will need to obtain permission directly from the copyright holder. To view a copy of this licence, visit <http://creativecommons.org/licenses/by-nc-nd/4.0/>.

© The Author(s) 2025